Polarization insensitive single mode Al$_2$O$_3$ rib waveguide design for applications in active and passive optical waveguides

A. Özden   Anadolu University, Faculty of Engineering, Department of Materials Science and Engineering, 26555 Eskişehir, Turkey

M. Demirtaş   Anadolu University, Faculty of Engineering, Department of Electrical and Electronics Engineering, 26555 Eskişehir, Turkey

F. Ay   Anadolu University, Faculty of Engineering, Department of Electrical and Electronics Engineering, 26555 Eskişehir, Turkey
feridunay@anadolu.edu.tr

Both passive and active, single mode, wavelength and polarization insensitive design of Al$_2$O$_3$ rib waveguides on SiO$_2$ substrate is reported. Influence of the waveguide height, etch depth, waveguide width and operation wavelength to the mode number, mode size, birefringence and polarization sensitivity were analyzed with Beam Propagation Method. Design parameters for targeted properties are computed for waveguide widths ranging from 0 to 10 μm, and for etch depth ranging from 0 to 0.5 μm for fixed waveguide height of 0.5 μm. A design window for a fixed width of 3.5 μm and etch depths between 0.325 to 0.375 μm is identified for single mode, wavelength and polarization insensitive operation of Al$_2$O$_3$ waveguides on thermal oxide. A novel rib TE mode selective filter design is also suggested as an output of the numerical simulations.
[DOI: http://dx.doi.org/10.2971/jeos.2015.15005]

1 INTRODUCTION

Al$_2$O$_3$ material recently has been a subject of special attention in the photonics community due to its superior mechanical and optical properties [1]. Amorphous Al$_2$O$_3$ (a-Al$_2$O$_3$) films are of interest for integrated optical circuits for several reasons. The refractive index is high compared with other oxide materials used in optoelectronic applications. Refractive index can be tuned between 1.62 and 1.68 with different deposition conditions without any additional doping [2]. Moreover, Al$_2$O$_3$ is an excellent host material for rare-earth ions and transition metal dopants [1]. Large amount of rare-earth ions can be homogeneously distributed into the Al$_2$O$_3$ matrix. This capability is of interest for realization of integrated optical amplifiers such as active waveguides. Furthermore, Al$_2$O$_3$ films show excellent transparency from UV to mid-IR range and have also been used in integrated optics for telecommunication wavelengths from 1.48 to 1.61 μm [1]. High quality a-Al$_2$O$_3$ are reported with different deposition methods such as d.c. planar sputtering [3], r.f. sputtering [4], chemical vapor deposition [5], pulsed laser deposition [6] and atomic layer deposition (ALD) [7]. ALD has several advantages over other deposition techniques. ALD is surface controlled method whereby other deposition techniques represent source controlled methods. In source controlled methods, the precursors react with each other before reaching with the target surface. This prevents monolayer growth and limits surface uniformity. Furthermore, ALD has the ability of large area deposition, in principle without any limitations as the maximum growth area depends only on the ALD chamber size [8]. ALD growth results in excellent conformity and reproducibility. Moreover, low temperature deposition is pos-

sible with highly reactive precursors. In addition, ALD allows deposition of different materials in a single process. The weak point of ALD is its slow growth rate, resulting in extended growth time. This problem can be tolerated by using a large chamber that contains many substrates [8]. As a result, ALD is an interesting growth method with a very high potential for waveguide applications.

In integrated optics optical ridge/rib structure is widely used in waveguide applications for active and passive optoelectronic devices. For most of the applications in photonics, the optical waveguides operate at single mode condition. In general, in order to fulfill this requirement, ridge waveguides are employed and designed with different numerical methods such as mode matching method [10], beam propagation method (BPM) [11], finite element method [12] and effective index method [13]. Design optimization studies on a variety of different material systems including SOI [14], GeSi [10], Si nanocrystal sensitized Er-doped SiO$_2$ [15] and a range of dielectrics [12] have already been reported. However, these studies do not focus on optimization of single mode a-Al$_2$O$_3$ based waveguide structure and polarization filtering action. Furthermore, experimental studies do not provide a design optimization of a-Al$_2$O$_3$ for single-mode ridge waveguide [7, 9]. Consequently, this study will focus to fulfill these objectives. A mode solver program is used based on BPM in order to optimize these parameters for a-Al$_2$O$_3$ core on SiO$_2$ substrates.
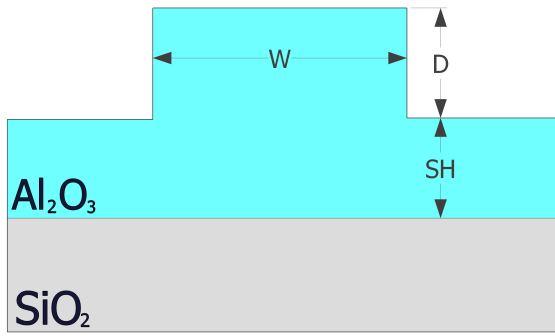
FIG. 1 Schematic of the simulated Al_2O_3 rib waveguide structure. D, W and SH represents etch depth, waveguide width and slab height, respectively.
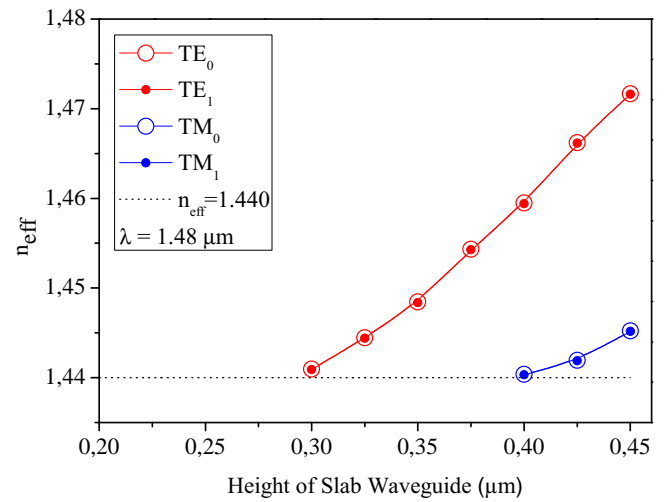

FIG. 2 Change of effective index (n_{eff}) with respect to slab height of the waveguide at λ = 1.48 μm. Fundamental and higher order modes were represented by open and filled circles, respectively. Red indicates TE polarization, and blue represents TM polarization. Dashed line indicates effective index value equal to substrate's (SiO_2) refractive index.

2 SIMULATION STRUCTURE AND SIMULATION PARAMETERS

The dimensions of the ridge waveguide structure investigated in this study are given in Figure 1. Al_2O_3 rib waveguide is on SiO_2 substrate. The refractive index value of amorphous Al_2O_3 at wavelength of 1.55 μm is known to be n = 1.64 [2] and that of SiO_2 is 1.44 [16]. W represents the width of the waveguide, H is the total thickness, D is the etch depth, and SH is the slab height of the rib waveguide. Since H is fixed to 0.5 μm, D is defined as $(0.5 - SH)$.

Total thickness of the rib waveguide was determined according to the ALD growth time and thickness limitation as explained in the introduction. Waveguide width is scanned from 0 to 10 μm with 0.2 μm increments. 0.2 μm was chosen as it represents the lateral resolution limitation of a general photolithography process. D is scanned between 0 to 0.5 μm with 25 nm increments. Zero D indicates a slab waveguide geometry with a SH of 0.5 μm. 0.5 μm D indicates photonic wire geometry.

Computation was performed with semi-vectorial Beam Propagation Method (BPM). In this technique, exact wave equation is approximated for monochromatic waves and then its numerically solved for guided wave problem by the BPM algorithm. One can find excellent reviews in the literature for the details of the technique and its variations [17]−[19]. To perform BPM, a simulation window of -50 μm to +50 μm in lateral direction, and -8 μm to +2 μm in vertical direction, and 5 mm waveguide length to satisfy convergence of the iterative mode solver was used. To prevent artificial back reflection of light incident on the boundary, Transparent Boundary Condition is used (TBC). Details of the TBC can be found elsewhere [20].

The position of the launched tilted fiber mode was adjusted as half of the width used in each run of the computation to excite possible higher order modes.

Birefringence resulting from the effective index change due to the Transverse Electric (TE) and Transverse Magnetic (TM) polarizations was calculated for three wavelengths of, 1.48, 1.53, and 1.55 μm. Birefringence caused by group index (n_g) was

also studied by using Eq. 1 [14],

$$n_g = n_{eff} - \lambda \times \frac{\delta n_{eff}}{\delta \lambda} \qquad (1)$$

where n_{eff} is the effective index at wavelength λ.

3 RESULTS AND DISCUSSION

In this section, analysis of one of the geometrical limits, i.e. the slab waveguide, will be discussed first. After obtaining required data from the slab waveguide, results of the rib waveguide are presented. Analyzed aspects of the rib waveguide includes single mode zone of the rib waveguide at different wavelengths, mode size of the selected rib waveguides and calculated birefringence of the selected rib waveguides.

3.1 a-Al_2O_3 slab waveguide

The aim of the slab waveguide analysis is to determine the thickness, SH, where the slab waveguide does not support any mode. This information is also used to support rib waveguide analysis. Investigated wavelengths are 1.48 μm (excitation wavelength of Er doped amplifier), 1.53 and 1.55 μm emission wavelengths of the amplifier. 1.61 μm at the border of third communication window also selected for simulation to see how far we can engineer the mode profile variation or to see the wavelength dependence of the single mode region of the waveguide.

The results of the numerical analysis of the slab waveguide are plotted in Figure 2. The graph demonstrates effective index (n_{eff}) values of both TE and TM polarizations at λ = 1.48 μm for different slab heights (SH). Dashed line indicates substrates (SiO_2) refractive index. It is well known that when the effective index of the waveguide decreases below the substrates refractive index, waveguide doesnt support any mode [21]. This fact can be observed in Figure 2. The minimum SH that support a mode is 0.30 μm for TE polarization
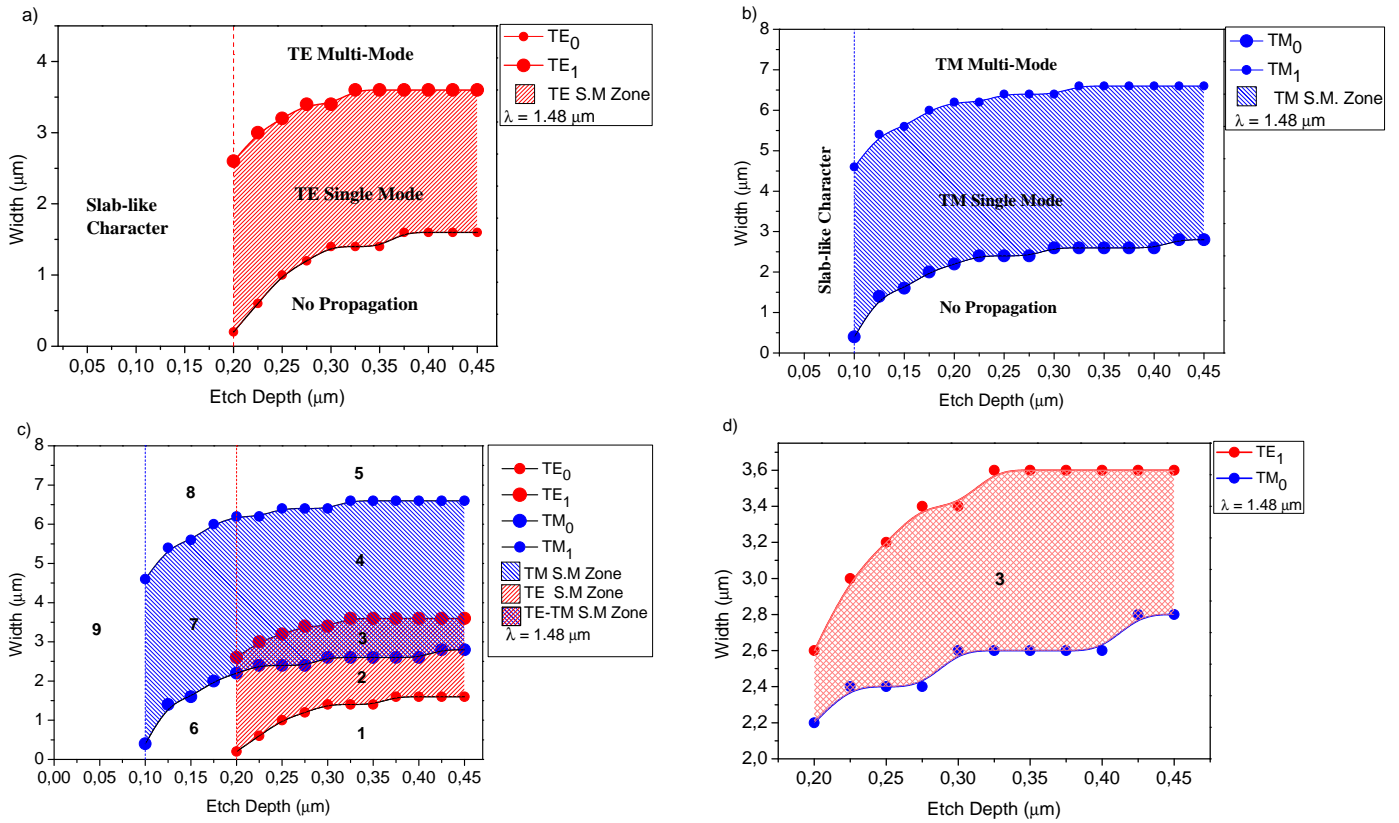
FIG. 3 Mode profile variation of rib waveguide as a function of width and etch depth at λ = 1.48 μm. Points represent cutoff dimensions of specific modes indicated in each figure. a) TE polarization, b) TM polarization, c) TE and TM polarizations, d) Single mode region for both polarizations, simultaneously. Numbers indicate special mode zones that are designated as in Table 1. Solid lines are to guide the eye.

and 0.40 μm for TM polarization. *SH* smaller than these values corresponds to n_{eff} values below the dashed line in Figure 2.

3.2 Mode analysis of rib waveguide

The rib waveguide mode analysis was performed for λ = 1.48, 1.53, 1.55 and 1.61 μm to identify the region with single mode propagation only. Each point in Figure 3 represents a special geometry where mode character of the rib waveguide changes. Depending on the geometry of the waveguide n_{eff} changes. As explained in section 3.1, n_{eff} values smaller than substrate refractive index result no light propagation. For example, for TE polarization at λ = 1.48 μm smaller red dots in Figure 3(a) corresponds to these rib geometries where this transition, no propagation to single mode propagation, occurs.

As an example, D = 0.25 and W = 1 μm is one of these geometries and supports only single mode. If we keep D constant and change the width of the rib waveguide to 0.8 μm, we end up with a waveguide that has no guiding. Therefore, these smaller red points can be considered as elements of a line separating two regions as single mode region and no propagation region in Figure 3(a), which also applies to TM polarization in Figure 3(b).

For a specific geometry the waveguide starts to support not only single mode but more than one mode. Consider the point representing D = 0. 25 μm and W = 1 μm in Figure 3(a). If we increase the width of the waveguide, it conserves its single mode character up to a point where it starts to support

TE$_1$. This special point is 3.2 μm for D = 0.25 μm, indicated by bigger red dot in Figure 3(a). Rest of the bigger red dots in Figure 3(a) correspond to a rib geometry where we have TE$_0$ and TE$_1$ simultaneously propagating in the waveguide. These points form a line that separates multi-mode region and single mode region. Same applies to Figure 3(b) for TM polarization (small blue dots).

It is apparent from Figure 3(a) and Figure 3(b) that there exist a range of width values for the fixed etch depth where the waveguide has single mode character. When combined, these ranges of width values form a single mode zone. Dashed red region in Figure 3(a) is the single mode region of TE mode and dashed blue region is single mode region for TM.

Beside the horizontal separation lines in Figure 3(a) and Figure 3(b), rib waveguides show a very interesting property that reveals itself by dashed vertical lines in same figures. Position of the vertical dashed lines are at D = 0.2 μm (0.3 μm slab height) and D = 0.1 μm (0.4 μm slab height) for TE and TM polarizations, respectively. Left hand side of the dashed lines indicates an area where one can always find a mode. We labeled this region as slab-like character in Figure 3(a) and 3(b). Slab waveguide analysis in Section 3.1 helps us to understand the slab-like character of the rib waveguide. When D goes to zero, etch depth of the waveguide gets smaller and slab height start to dominate the character of the rib waveguide. We found that a rib waveguide with slab height of 0.3 μm for TE and 0.4 μm for TM polarization behaves like a slab waveguide. Please note that exactly same slab thicknesses also found in slab waveguide analysis in Section 3.1 demonstrat-

Region Number	Waveguide Propagation Characteristics
1	No propagation zone for both polarizations
2	Single mode propagation for TE and no propagation for TM.
3	Single mode region for both polarizations.
4	Single mode for TM and multi-mode for TE.
5	Multi-mode for both polarizations.
6	Slab-like character for only TE and no propagation for TM.
7	Single mode for TM and slab like character for TE mode.
8	Multi-mode for TM and slab like character for TE mode.
9	Slab-like character for both polarizations.

TABLE 1 Combination of mode profiles of TE and TM polarizations designate nine different regions that demonstrate "propagation characteristics" of the waveguide of which two of them (number 2 and 3) are technologically important. Please note that region number 3 in bold is the single mode region for both polarizations.

ing guiding geometry above these critical thicknesses. In the case of slab waveguide these thicknesses are found to be critical. Below these thicknesses there was no mode for the slab waveguide. However, for thicker slab dimensions multi-mode character is observed. In the rib waveguide case, above these slab thicknesses waveguide has multi-mode character without any width dependence. The interesting point here is that this change of the behavior from rib to slab propagation is very sharp.

Simulations have been carried out to find a region where we have single mode character for both polarizations. It is possible to obtain this region by combining the data of two polarizations represented at Figure 3(a) and Figure 3(b). When combined together, Figure 3(c) is obtained. Combination has resulted in 9 different regions that are identified and designated in Table 1.

Figure 3(c) which is the combination of Figure 3(a) and 3(b) demonstrates the flexibility of a rib waveguide that gives many important technological features by just changing two simple and easily achievable parameters, *D* and *W* with photolithographic processes. In Figure 3(c) we have nine regions. These regions are labeled from 1 to 9 in Figure 3(c). Numbers are explained in Table 1. Two of them are technologically important. Importance of single mode region (region number 3) was explained in the introduction and also Figure 3(d) demonstrates the region number 3 in detail. There is an additional region that is labeled with 2. Rib waveguide geometry that falls into this area does not allow TM polarization to propagate but guides TE polarization only. Therefore, this region filters out the incident TM polarization and hence transmits only the TE polarization. Such a waveguide can be used as a TE mode selective filter.

Mode selective filters are basic devices for communication and optical sensing applications [22]. To the best of our knowledge, there is no report on such a simple rib waveguide filter device in literature. Most of the TE mode selective filters fabri-
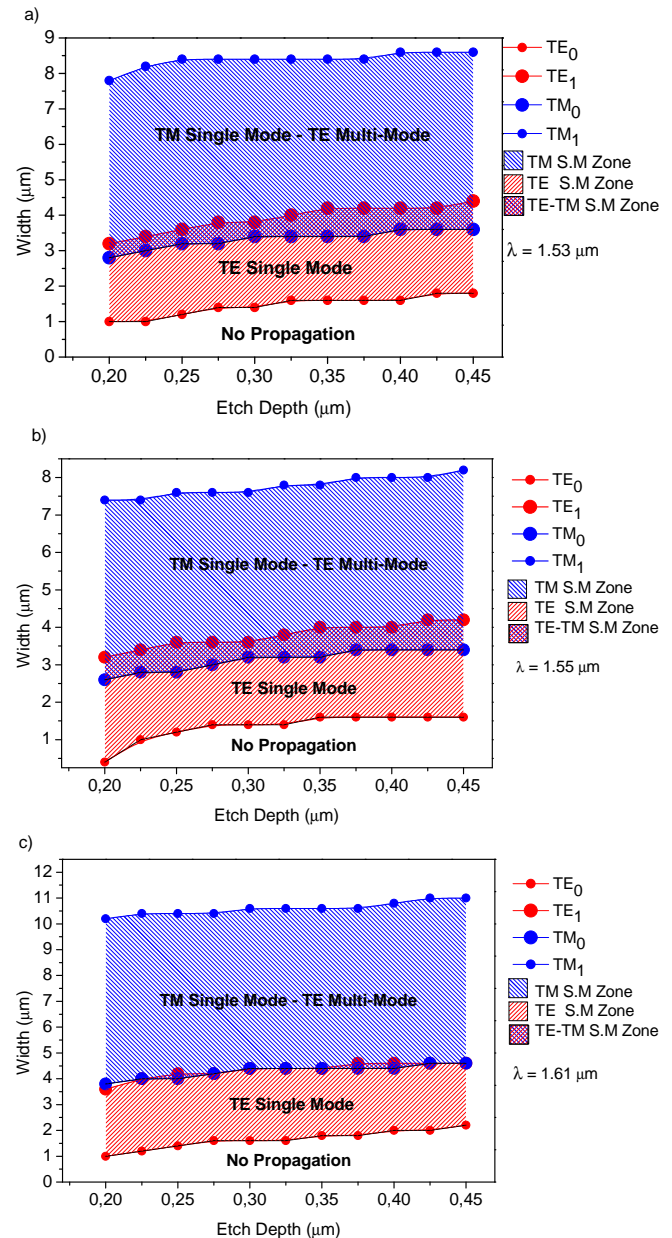

FIG. 4 Mode regions for the third optical communication window at a) $\lambda = 1.53$ μm, b) $\lambda = 1.55$ μm, and c) $\lambda = 1.61$ μm. S.M in the legends is acronym for "single mode".

cated have much more complex structures than demonstrated in this article. For instance, one waveguide structure that filters the TM mode uses metal claddings and hence called as metal-clad optical waveguides [23]. It benefits the higher loss of TM mode in metal cladding [23, 24]. There are also waveguides that benefit from anisotropy of the materials for filtering [25]. A device that benefits from such effects requires additional layers [26] or different materials that are hardly compatible with each other making integration and fabrication process complicated. Here we suggest a possible TE mode selective filter using amorphous Al_2O_3 rib waveguide that has no metal claddings, no additional buffer layers [26] to leak TM mode or has no anisotropy due to the amorphous nature. The only requirement is that both the waveguide width and etch depth of the rib structure must be selected from TE single mode region of Figure 3(c). *W* and *D* can be easily adjusted with well-known standard photolithography process.

The idea of the rib waveguide mode selective filter can be gen-
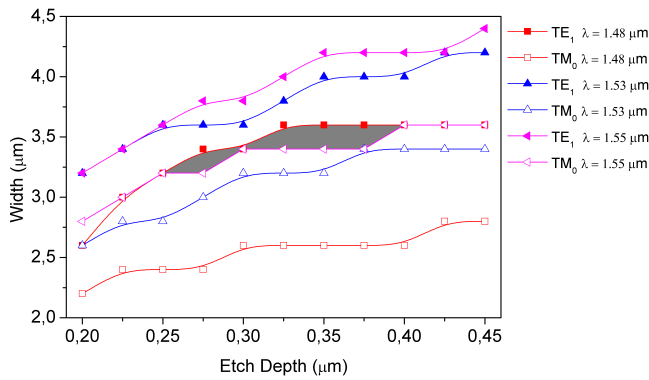
FIG. 5 Gray shaded area demonstrates the region where indicated wavelengths are single mode without any polarization dependence. Solid lines are to guide the eye.

FIG. 6 Selected geometries for mode size investigation at different wavelengths.

eralized for amorphous oxide materials that have total thickness less than operation wavelength with a moderate refractive index change (n), which is around 0.2.

The idea of identifying a polarization insensitive single mode region for the rest of the wavelengths was also tested. Figure 4 gives these regions for the rest of the wavelengths. It must be noted that the cross section of the TE and TM single mode region gives technologically important area only above $D = 0.2$ μm. Therefore, the data including regions 6 to 9 that was labeled in Figure 3(c) and explained in Table 1 was omitted for the rest of the wavelengths.

Inspection of Figure 4 indicates that increase of the wavelength results in shrinkage of the polarization insensitive region. At 1.61 μm the region collapses to a line. In principle, simulations suggest that its still possible to work in a single mode region, if W and D are selected exactly on this line, however it may not be practical due to the resolution of lithography process and fabrication tolerance limits.

In addition to polarization insensitive single mode region, we can identify a region that is also wavelength insensitive. This can be done by merging graphs of Figure 3(c), Figure 4(a), Figure 4(b) and Figure 4(c). Figure 5 gives the resulting zone.

Combination of mode profiles of all wavelengths including polarization effects do not provide a polarization and wavelength single mode insensitive region for 1.61 μm, but ensures the targeted characteristics for the rest of the wavelengths as depicted in Figure 5. On the other hand, the geometries in shaded gray area in Figure 5 can be used for Erbium doped Al_2O_3 optical amplifiers, which are pumped at 1.48 μm and have an emission wavelength of 1.53 and 1.55 μm [27, 28].

The shaded area in Figure 5 indicates another special region of the rib waveguide. Once again by selecting W and D properly, one can design a rib waveguide that supports three wavelengths or a range of wavelengths from 1.48 μm to 1.55 μm ensuring single mode propagation without any polarization restriction. Considering the fabrication tolerances of the photolithography fabrication process the suggested target dimensions range is between a ridge width of 3.5 μm and D of 325 nm to 375 nm.
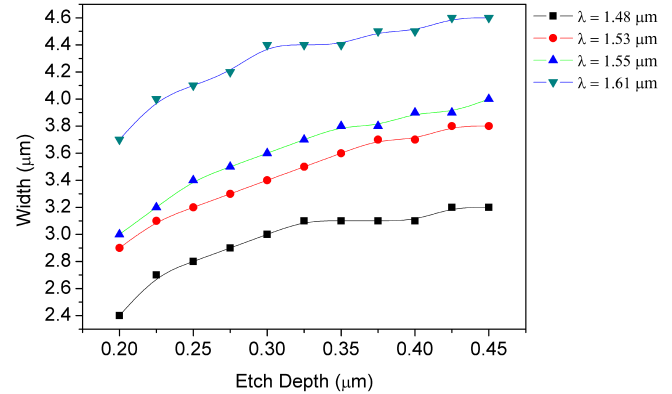
3.3 Mode size of rib waveguide

Mode sizes of the selected rib waveguides were investigated. Mode size in this investigation is defined as the width that corresponds to $1/e$ of the peak intensity at both x and y direction, labeled as W_x and W_y, respectively. Here we use mode area concept that gives rough but better evaluation of the confinement. Mode area is defined by simple multiplication of W_x and W_y. Geometry selection criteria depend on the limitation of the lithography process. A set of data points that forms a line at half of the single mode region is selected. Results for these geometries are given in Figure 6 for each wavelength.

Mode area of the rib waveguides with selected geometries are depicted in Figure 7. The mode area is given for different wavelengths and polarizations. The results at $\lambda = 1.48$ μm are given in Figure 7(a) for TE and 7(b) for TM polarization, 1.55 μm are given in Figure 7(c) for TE and 7(d) for TM and finally 1.61 μm are given in Figure 7(e) for TE and 7(f) for TM polarization.

Inspection of the Figure 7 for the geometries of interest leads to the following observations:

- Longer wavelengths always result in a larger mode area than shorter wavelengths.

- TM polarization always gives bigger mode area than TE polarization.

- Mode area slightly decrease when etch depth gets deeper and width gets wider.

Mode area can be thought as an indication of the confinement. It is apparent that frequency of the longer wavelength would be relatively close to cutoff frequency with respect to shorter ones. As we approach to cutoff frequency, mode confinement at the Al_2O_3 layer decreases and evanescent field expands. This expansion corresponds to bigger mode area.

In the BPM method that we use, we always monitor electric field profile. Electric field is along X direction (vertical direction) for TE polarization. In this direction, maximum boundary dimension that field encounters is the total waveguide height which is 0.5 μm thick. In the case of TM polarization,
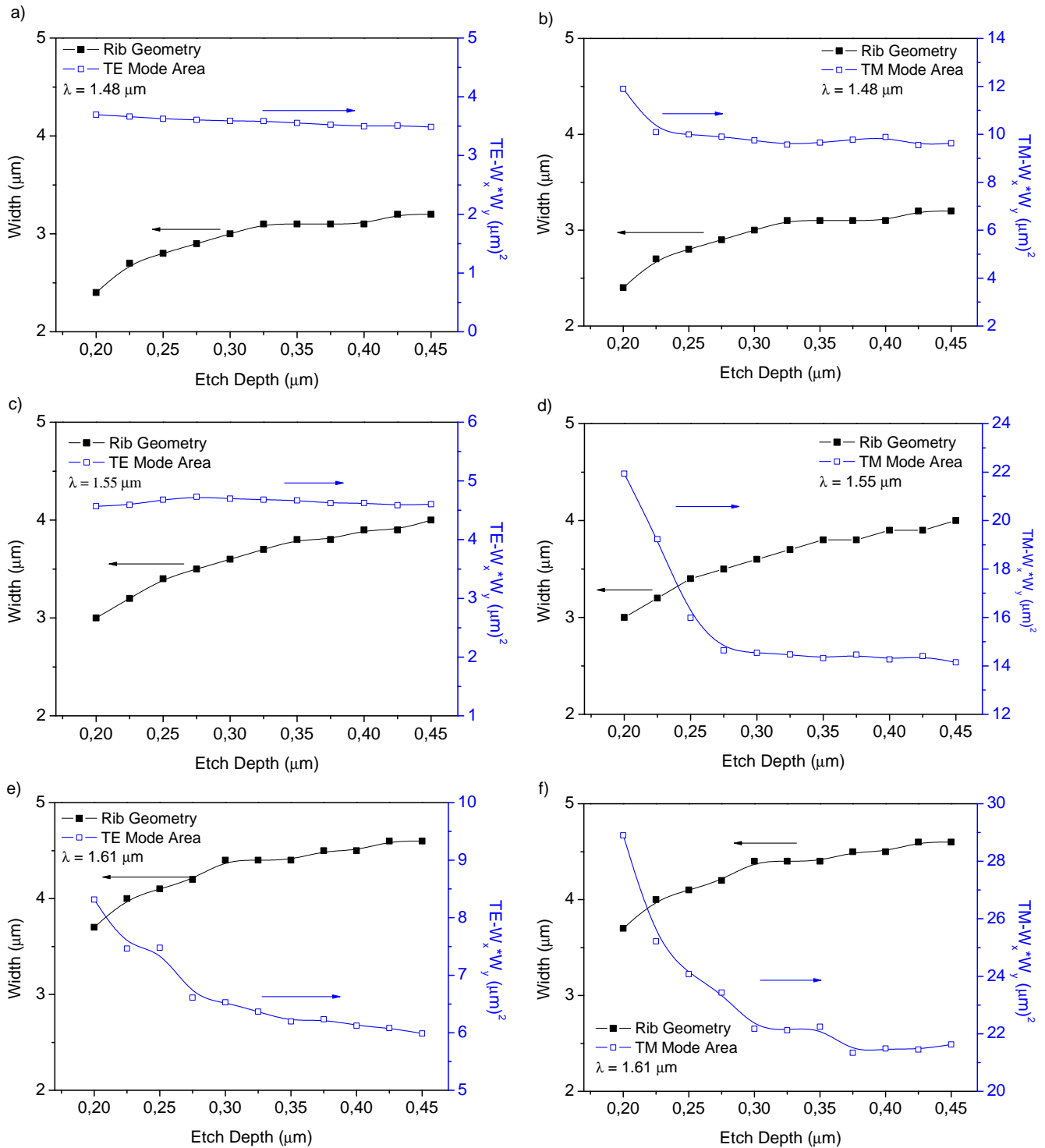
FIG. 7 Mode areas of the three wavelengths as a function of rib geometries. a) 1.48 μm-TE, b) 1.48 μm -TM, c) 1.55 μm - TE, d) 1.55 μm - TM, e) 1.61 μm-TE, f) 1.61 μm - TM. Geometry can be read from filled squares. Mode area can be read via open blue squares from second Y axis.

electric field is along Y direction (lateral direction). Lateral direction includes width, which is 5 to 6 times larger than total height. We have also an extended slab thickness of the rib waveguide in this direction. Therefore, the electric field of TM polarization is much larger than TE and to fulfill boundary conditions mode size has to be larger than TE polarization. Effective index method was also used to reach the same conclusion.

Confinement of the single mode region was also evaluated for 1.55 μm due to the importance of this wavelength. It is also done to evaluate our observation on the general mode area

trend as given above (result number 3). Confinement was calculated by numerically integrating the total area of the three dimensional mode intensity on X-Y plane. Result can be seen in Figure 8(a).

TE confinement starts from 49.57% for smallest single mode dimension and increases up to 51.47% as *D* and *W* both gets larger. Relatively low confinement factor can be assigned to the small ridge height with respect to launched wavelength. Mode profiles were also given in Figure 8. Figure 8(b) and 8(c) depicts electric field profiles for TE polarization and Figure 8(d) gives electric field profile for TM polarization.
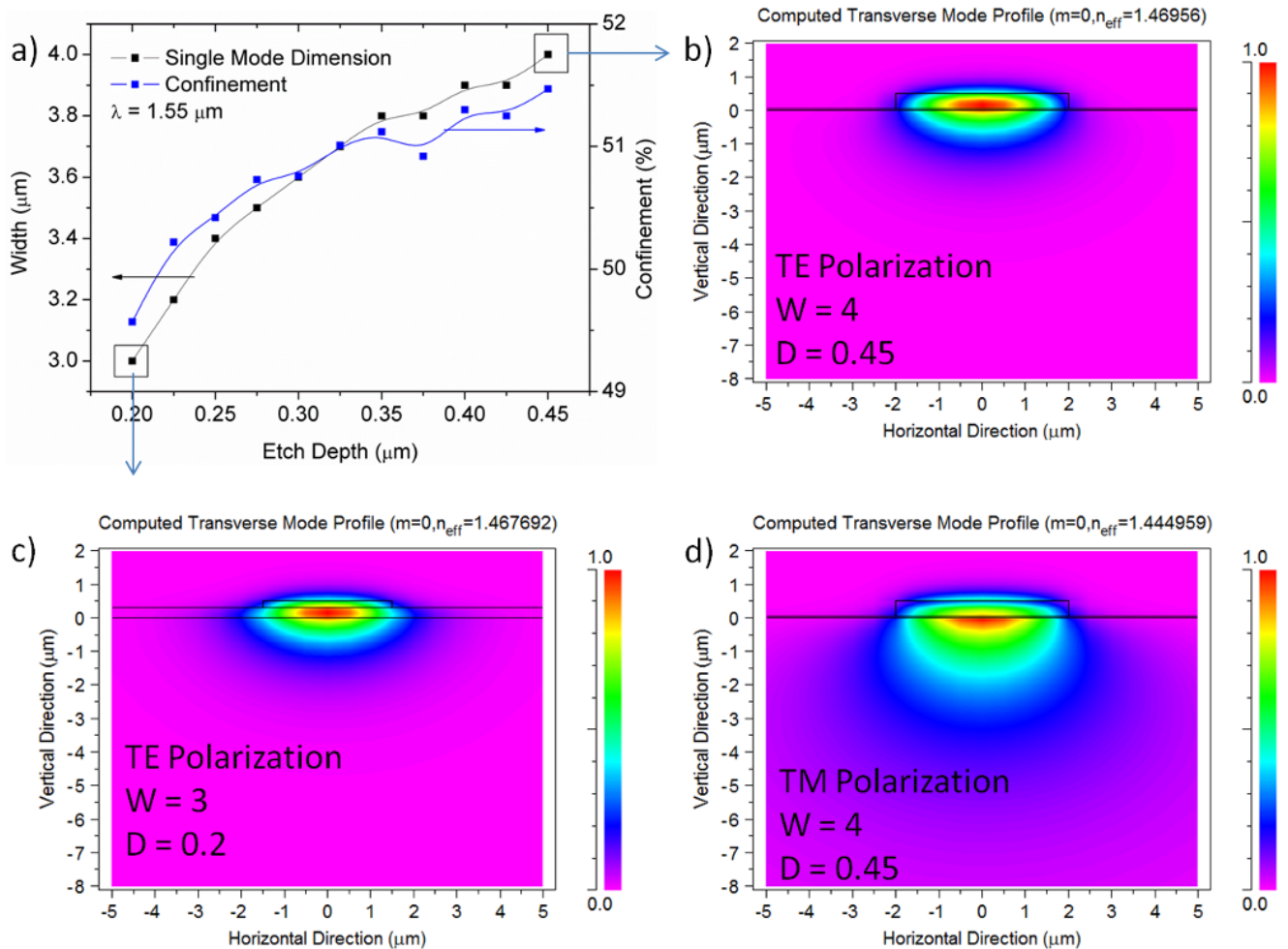
FIG. 8 Single mode confinement of the rib waveguide with respect to W and D at $\lambda = 1.55$. a) Confinement factor for different geometries, b) TE mode field profile at $W = 3$ and $D = 0.2$, c) TE mode field profile at $W = 4$ and $D = 0.45$, d) TM mode field profile at same dimension with c.

The rib waveguide reported in Figure 8(c) has $W = 3$ μm and $D = 0.2$ μm with a slab height of 0.3 μm. The rib waveguide at Figure 8(b) has $W = 4$ μm and $D = 0.45$ μm with a very thin slab thickness of 0.05 μm. Close inspection of Figure 8(b) and 8(c) gives important aspects for possible active waveguide applications. Location of the peak intensity is important for the excitation of all the active ions. The location of the peak of the electric field intensity is just above the 50 nm thick slab of the rib waveguide. Therefore its inside the ridge for the Figure 8(b) whereas the peak position of the electric field intensity is inside the 300 nm slab part of the rib waveguide for the geometry depicted in Figure 8(c). Although the two structure have almost the same confinement factors, larger width and deeper etch depth is much preferable for amplification application due to the mode intensity distribution profile. In the case of TM polarization, field profile looks much wider than TE as shown and explained in Figure 7. Finally, the horizontal field spread both for TE and TM polarization is observed to be limited.

3.4 Rib waveguide birefringence

For the shaded area indicated in Figure 5, there exists no zero birefringence rib waveguide geometry. For a fixed width bire-

fringence decreases with increasing etch depth for neff and it makes a minimum at $D = 0.33$ μm for Δn_g which are shown in Figure 9(a) and Figure 9(b). Same trends are also observed for individual single mode regions. This is due to the fact that TE is well confined within the investigated geometries, which means effective index of the TE mode is quite higher than substrate index (around 1.47). This better support of TE modes can be also seen in mode area in Figure 7 and mode confinement in Figure 8. On the other hand, TM is barely supported by the geometries where we have one single mode and wavelength independence. In addition, much larger mode area indicates a lower effective index. Effective indexes of these geometries are just above 1.444 for TM polarization. These relatively large split between effective indexes results in exclusion of zero birefringence character of the waveguide in the range of simulated wavelength and polarization insensitive design geometries.

4 CONCLUSION

Polarization insensitive single mode design of Al_2O_3 rib waveguide has been presented for four wavelengths of 1.48, 1.53, 1.55 and 1.61 μm. Numerical simulations suggested use
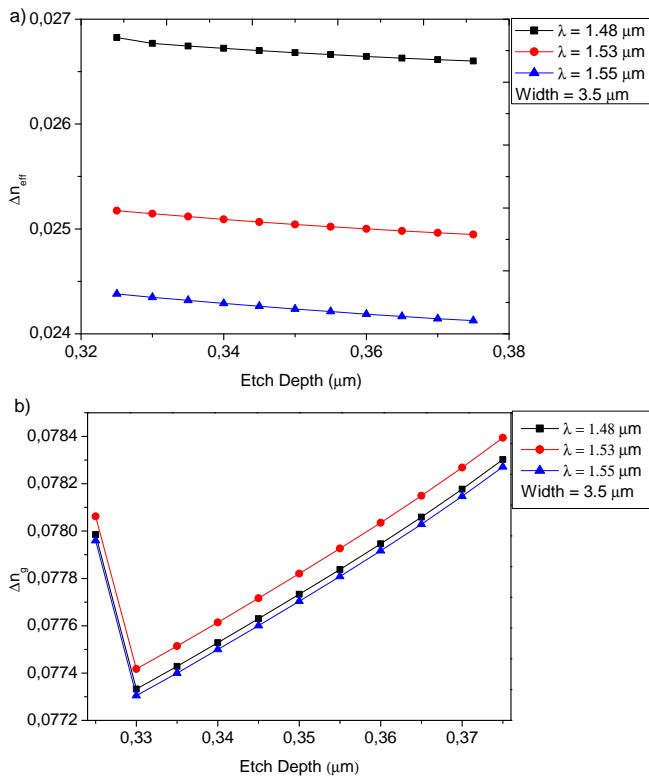
FIG. 9 Δn_{eff} and Δn_g calculated for the shaded area in Figure 5 as a function of D.

of a design window of 3.5 μm ridge width with 325 nm to 375 nm etch depth for wavelength insensitive single mode rib waveguides for the wavelengths of 1.48, 1.53 and 1.55 μm.

It is suggested to use deeply etched profiles and wide width rib waveguides to achieve better confinement and to have a useful mode intensity distribution for amplification applications. As a result of the calculations, it was determined that there is no zero birefringence design for 0.325 to 0.375 μm etch depth for fixed width of 3.5 μm in range for wavelength insensitive region and that it is not possible to compensate birefringence by changing the geometry of the rib waveguide at this range.

Numerical simulations suggested a possible rib waveguide TE mode selective filter. Novelty of this filter is its simplicity in fabrication over its counterparts. Filtering mechanism depends only on the etch depth and width of the rib waveguide. For future study, enlargement of the wavelength insensitive single mode region and increase of the confinement will be targeted by applying different designs. Experimental realization of rib TE mode selective filter is to be implemented. Moreover, possible TM mode selective filter will be considered with the same approach.

5 ACKNOWLEDGMENTS

References

[1] S. Kasap, and P. Capper *Springer Handbook of Electronic and Photonic Materials* (Springer, New York, 2006).

[2] M. Demirtaş ,A. Özden, and F. Ay, "Optimization of ALD grown Al$_2$O$_3$ host material for use in integrated optical circuits," *in proceedings to the 10th Nanoscience and Nanotechnology Conference* 138 (Yeditepe University, Istanbul, 2014).

[3] G. Este, and W. D. Westwood, "Reactive deposition of low loss Al$_2$O$_3$ optical waveguides by modified dc planar magnetron sputtering," J. Vac. Sci. Technol. A **2**, 1238 (1984).

[4] M. K. Smit, and G. A. Acket, "Al$_2$O$_3$ films for integrated optics," Thin Solid Films **138**, 171–181, (1986).

[5] M. Mahnke, S. Wiechmann, H. J. Heider, O. Blume, and J. Müller, "AluminumOxide Doped with Erbium, Titaniumand Chromiumfor Active Integrated Optical Applications," Int. J. Electron. Comm. **50**, 342–348 (2001).

[6] A. Suarez-Garcia, J. Gonzalo, and C. N. Afonso, "Low-loss Al$_2$O$_3$waveguides produced by pulsed laser deposition at room temperature," Appl. Phys. A-Matter **77**, 779–783 (2003).

[7] M. M. Aslan, N. A. Webster, C. L. Byard, M. B. Pereira, C. M. Hayes, R. S. Wiederkehr, and S. B. Mendes, "Low-Loss Optical Waveguides for the Near Ultra-Violet and Visible Spectral Regions with Al$_2$O$_3$ Thin Films from Atomic Layer Deposition," Thin Solid Films **518**, 4935–4940 (2010).

[8] H. Moshe, and Y. Mastai, "Atomic Layer Deposition on Self-Assembled-Monolayers," in *Materials Science - Advanced Topics*, Prof. Yitzhak Mastai (Ed.) (InTech, Rijeka, 2013).

[9] K. Solehmainen, M. Kapulainen, P. Heimala, and K. Polamo, "Erbium-Doped Waveguides Fabricated With Atomic Layer Deposition Method," IEEE Photonic Tech. L. **16**, 194–196 (2004).

[10] R. A. Soref, J. Schmidtchen, and K. Petermann, "Large Single-Mode Rib Waveguides in GeSi-Si and Si-on-SiO$_2$," IEEE J. Quantum Elect. **27**, 1971–1974 (1991).

[11] N. M. Kassim, A. B. Mohammad, A. S. M. Supa'at, M. H. Ibrahim, and S. Y. Gang, "Single Mode Rib Optical Waveguide Modeling Techniques," *in proceedings of RF and Microwave Conference Malaysia*, 272–276 (IEEE, Subang, Selangor, 2004).

[12] M. Laurentis, A. Irace, and G. Breglio, "Determination of single mode condition in dielectric rib waveguide with large cross section by finite element analysis," J. Comput. Electron. **6**, 285–287 (2007).

[13] J. Duan, J. Wang, B. Zhang, and Y. Ren, "Optimizing Design of a Single-Mode Optical Rib Waveguide," Adv. Mat. Res. **710**, 464–468 (2013).

[14] L. Vivien, S. Laval, B. Dumont, S. Lardenois, A. Koster, and E. Cassan, "Polarization-independent single-mode rib waveguides on silicon-on-insulator for telecommunication wavelengths," Opt. Commun. **210**, 43–49 (2002).

[15] C. Ciminelli, P. Frascella, and M. N. Armenise, "Optical modelling of a Si-based DBR laser source using a nanocrystal Si-sensitized Er-doped silica rib waveguide in the C-band," J. Eur. Opt. Soc.-Rapid **3**, 08017 (2008).

[16] M. Bass, C. DeCusatis, J. Enoch, V. Lakshminarayanan, G. Li, C. MacDonald, and V. Mahajan et al., *Handbook of optics* (3rd edition, McGraw Hill Professional, London, 2009).

[17] R. Scarmozzino, A. Gopinath, R. Pregla, and S. Helfert, "Numerical techniques for modeling guided-wave photonic devices," IEEE J. Sel. Top. Quant. **6**, 150–162 (2000).

[18] D. A. Yevick, "guide to electric-field propagation techniques for guided-wave optics," Opt. Quant. Electron. **26**, S185–S197 (1994).

[19] K. S. Chiang, "Review of numerical and approximate methods for the modal analysis of general optical dielectric waveguides," Opt. Quant. Electron. **26**, S113–S134 (1994).

[20] G. R. Hadley, "Transparent boundary condition for the beam propagation method," IEEE J. Quantum Electron. **28**, 363–370 (1992).

[21] C. R. Pollock, *Fundamentals of Optoelectronics* (Richard D Irwin Inc, Chicago, 1994).

[22] O. Watanabe, M. Tsuchimori, A. Okada, and H. Ito, "Mode selective polymer channel waveguide defined by the photoinduced change in birefringence," Appl. Phys. Lett. **70**, 750–752 (1997).

[23] S. Ohke, T. Umeda, and Y. Cho, "TM-mode selective filter using leaky waveguide structure," Electron. Commun. JPN. **85**, 1241–1246 (2002).

[24] Y. Suematsu, M. Hakuta, K. Furuya, K. Chiba, and R. Hasumi, "Fundamental transverse electric field (TE0) mode selection for thin-film asymmetric light guides," Appl. Phys. Lett. **21**, 291–293 (1972).

[25] Y. Okamura, S. Yamamoto, and T. Makimoto, "Wave propagation in semileaky-type anisotropic thin-film optical waveguides," J. Opt. Soc. Am. **67**, 539–545 (1977).

[26] A. Y. Agapov, A. P. Gorobetz, V. M. Shevtsov, and P. M. Zhitkov, "Efficient TM-pass multilayer planar optical waveguide polarizer," Electron. Lett. **27**, 1804–1805 (2012).

[27] G. N. V. D. Hoven, R. J. I. M. Koper, and A. Polman, "Net optical gain at 1.53 μm in Er-doped Al_2O_3 waveguides on silicon," Appl. Phys. Lett., **64**: 1886-1888, (1996).

[28] L. Agazzi, J. D. Bradley, M. Dijkstra, F. Ay, G. Roelkens, R. Baets, K. Wörhoff, et al., "Monolithic integration of erbium-doped amplifiers with silicon-on-insulator waveguides," Opt. Express **18**, 27703–27711 (2010).